Published in final edited form as:
Circulation. 2006 November 28; 114(22): 2342–2350.

X-Ray Fused With Magnetic Resonance Imaging (XFM) to Target Endomyocardial Injections: Validation in a Swine Model of Myocardial Infarction

Ranil de Silva, MRCP, PhD*, **Luis F. Gutiérrez, PhD***, **Amish N. Raval, MD**, **Elliot R. McVeigh, PhD**, **Cengizhan Ozturk, MD, PhD**, and **Robert J. Lederman, MD**
Cardiovascular Branchand Laboratory of Cardiac EnergeticsDivision of Intramural Research, National Heart, Lung, and Blood Institute, National Institutes of Health, Bethesda, Md; and the Department of Biomedical Engineering, Johns Hopkins University School of Medicine, Baltimore, Md

Abstract

Background—Magnetic resonance imaging (MRI) permits 3-dimensional (3D) cardiac imaging with high soft tissue contrast. X-ray fluoroscopy provides high-resolution, 2-dimensional (2D) projection imaging. We have developed real-time x-ray fused with MRI (XFM) to guide invasive procedures that combines the best features of both imaging modalities. We tested the accuracy of XFM using external fiducial markers to guide endomyocardial cell injections in infarcted swine hearts.

Methods and Results—Endomyocardial injections of iron-labeled mesenchymal stromal cells admixed with tissue dye were performed in previously infarcted hearts of 12 Yucatan miniswine (weight, 33 to 67 kg). Features from cardiac MRI were displayed combined with x-ray in real time to guide injections. During 130 injections, operators were provided with 3D surfaces of endocardium, epicardium, myocardial wall thickness (range, 2.6 to 17.7 mm), and infarct registered with live x-ray images to facilitate device navigation and choice of injection location. XFM-guided injections were compared with postinjection MRI and with necropsy specimens obtained 24 hours later. Visual inspection of the pattern of dye staining on 2,3,5-triphenyltetrazolium chloride–stained heart slices agreed (κ=0.69) with XFM-derived injection locations mapped onto delayed hyperenhancement MRI and the susceptibility artifacts seen on the postinjection T2*-weighted gradient echo MRI. The distance between the predicted and actual injection locations in vivo was 3.2±2.6 mm (n=64), and 75% of injections were within 4.1 mm of the predicted location.

Conclusions—Three-dimensional to two-dimensional registration of x-ray and MR images with the use of external fiducial markers accurately targets endomyocardial injection in a swine model of myocardial infarction.

Keywords

catheterization; interventional magnetic resonance imaging; mapping; myocardial infarction; stem cell therapy; stereotaxic techniques; radiography

Correspondence to Robert J. Lederman, MD, Cardiovascular Branch, Bldg 10, Room 2C713, Bethesda, MD 20892-1538. E-mail lederma r@nhlbi.nih.gov
*Dr de Silva and Dr Gutiérrez contributed equally to this work.

Disclosures
None.

Transcatheter endomyocardial injection may be an important route for delivery of emerging biological therapies such as cellular products,[1–8] plasmid,[9–14] and virus.[10] This route may be particularly important for treating myocardium supplied by an occluded epicardial coronary artery. The ability to target endomyocardial injections may facilitate local delivery of therapies to those myocardial regions where chances of efficacy are greatest and minimize the risk of injections into regions with thin myocardial walls.

Cardiac magnetic resonance imaging (MRI) provides precise noninvasive assessment of global and regional wall motion[15] and myocardial viability.[16] We have developed a novel method to register MR images of the heart with x-ray fluoroscopy using external fiducial markers.[17] In this study, we describe the use of this technique of x-ray fused with MRI (XFM) to perform targeted endomyocardial injections of iron-labeled mesenchymal stromal cells (Fe-MSC) in hearts of swine with prior myocardial infarction.

Methods

Animal Procedures

Animal procedures were approved by the National Heart, Lung, and Blood Institute Animal Care and Use Committee. Twelve Yucatan miniswine (weight, 33 to 67 kg; 5 male and 7 female) received aspirin, clopidogrel, and atenolol for 3 days before myocardial infarction. Anesthesia was induced with the use of atropine, butor-phanol, ketamine, and xylazine and maintained with the use of inhaled isoflurane and mechanical ventilation. After transfemoral arterial and venous access, animals received intravenous heparin (50 U/kg), amiodarone (300 mg), and lidocaine (0.5 to 1 mg/kg bolus plus 0.5 to 1 mg/min infusion). The goals of this study were to test the safety and accuracy of XFM-guided targeted endomyocardial injection in and around infarcted myocardium of varying size, age, and location. Myocardial infarction was induced by 45- to 90-minute balloon occlusion of either the left anterior descending (n=8) or left circumflex (LCX) (n=4) coronary arteries. Endomyocardial injection procedures were performed 3 to 74 days (median, 17.5) after the myocardial infarction procedure.

Preparation and Labeling of Mesenchymal Stromal Cells

Fe-MSC were prepared from bone marrow aspirates taken from 2 additional Yucatan miniswine. Ferumoxides (Feridex, Berlex Pharmaceuticals, Montville, NJ) labeling was facilitated by protamine sulfate.[18] Fe-MSC were resuspended at a final concentration of 2 to 4×10^6/mL in phosphate-buffered saline for injection.

Preinjection MRI Protocol

MRI was performed at 1.5 T (Sonata, Siemens, Erlangen, Germany) with an 8-channel phased-array surface coil (Nova Medical Inc, Wilmington, Mass). Images were acquired immediately preceding injection. Dual-modality x-ray and MRI–conspicuous fiducial markers (Beekley Corp, Bristol, Conn) were prepared containing 5 mmol/L gadopentetate dimeglumine (Gd-DTPA) (Magnevist, Berlex) and iodinated radiocontrast (iodixanol 320 mg I/mL; Visipaque, GE Healthcare, Oslo, Norway). In each animal, 15±1 external fiducial markers were secured to the thorax with adhesive dressings. All images were acquired during end-expiration. Endocardial and epicardial borders were defined from multiple, breath-held, ECG-gated cine steady state free precession (SSFP) MRI with the following parameters: repetition time (TR)/echo time (TE), 3.6/1.8 ms; flip angle, 65°; field of view (FOV), 300×244 mm; matrix, 256×127 pixels; slice thickness, 8 mm; bandwidth, 1085 Hz per pixel. Infarcts were visualized on delayed hyperenhancement (DHE) MRI images acquired 15 minutes after intravenous Gd-DTPA 0.2 mmol/kg with the use of a phase-sensitive inversion recovery sequence[19] with the following parameters: TR/TE, 11/4.45 ms; flip angle, 30°; inversion time, 300 ms; FOV, 350×241 mm; matrix, 256×141 pixels; slice thickness, 8 mm; bandwidth, 140 Hz per pixel.

Finally, a 3-dimensional (3D) T1-weighted gradient echo scan was performed to locate the external fiducial markers with the following parameters: TR/TE, 2.37/1.18 ms; flip angle, 17°; FOV, 400×300×230 mm; matrix, 256×192×61 voxels; bandwidth, 1300 Hz per pixel. Images were transferred to a Leonardo workstation (Siemens) for manual segmentation of endocardial and epicardial borders at end-diastole and end-systole from SSFP images; infarct borders from DHE images; and external fiducial markers from the 3D, T1-weighted gradient echo images. MRI gradient warping distortion was corrected with the use of a Siemens-supplied algorithm.[20]

XFM Registration Techniques

After MRI, the animals were transferred for x-ray (Axiom Artis FC, Siemens) with the use of a mechanized transport table that allows bidirectional transfer between the MRI and x-ray suites (Miyabe, Siemens). Single-phase MR images acquired at end-systole and end-diastole were registered to the live x-ray acquisitions as reported previously[17] and outlined in Figure 1. Briefly, fiducial marker locations in the x-ray and MR images were segmented to provide matching points within their respective coordinate systems. These were registered by minimizing the distance between matching fiducial marker locations with the use of a nonlinear least-squares optimization that iteratively fitted the 6 parameters (3 rotations and 3 translations) of a rigid body transformation. Image intensifier–associated distortions (pincushion and sigmoidal magnetic field) were corrected with empirical 2-dimensional (2D) fifth-order polynomials.[17]

B-spline tensors were fitted to the MR-derived contours to generate smoothed surfaces.[21] Myocardial thickness at end-diastole for each point in the endocardial surface was determined by computing the distance to the closest point on the epicardial surface and was displayed as a 3D surface map. The MR-derived surfaces were registered with the x-ray coordinate system as above and were then fused with live x-ray images during injections. Fusion images were presented to the operator as single-phase, end-diastolic, MR-derived surfaces superimposed on live x-ray fluoroscopy images displayed at 8 frames per second on a second display alongside the vendor's live x-ray display.

Endomyocardial Injection Procedures

Animals received heparin (50 U/kg), supplemented to maintain an activated clotting time >250 seconds. Expiratory breath-held left ventriculograms were acquired in left anterior oblique 45° and right anterior oblique 45° or anteroposterior projections on which the MR-derived surfaces of left ventricular epicardium, endocardium, and right ventricular endocardium were superimposed (Figure 2). Three-dimensional surfaces representing myocardial thickness and infarcted myocardium were used to define targets for endomyocardial injection with presumably low perforation risk (Figure 3A to 3D). Injection locations were considered safe if the wall thickness was >6 mm. We intended injections into both the center and borders of the infarcts. Injections were performed by experienced interventional cardiologists using the Stilletto endomyocardial injection system (Boston Scientific, Natick, Mass), a spring-loaded 26-gauge injection needle that extends 3.5 mm, positioned with coaxial 7F and 9F guiding catheters. The volume of each injection was 0.4 mL, including 20% tissue dye (TMD-5, Triangle Biomedical Sciences, Durham, NC). When technically possible, the injection needle was guided to a desired location on the basis of the MRI-determined infarct location. Otherwise, the closest region with appropriate wall thickness was targeted. Two orthogonal x-ray images were acquired during each injection to reconstruct the needle position in a 3D x-ray coordinate system. These were displayed to help avoid overlap (Figure 3).

Postinjection MRI Protocol

At the end of the injection procedure, animals were transferred for repeat MRI and to determine evidence of pericardial effusion. Diaphragmatic navigator–gated 3D T2*-weighted gradient echo (T2*W-GRE) imaging (TR/TE, 8.39/3.18 ms; flip angle, 10°; FOV, 250×250×88 mm; matrix, 256×256×88 voxels; bandwidth, 130 Hz per pixel) was performed to locate Fe-MSC. A 3D acquisition was repeated to locate external fiducial markers. Animals recovered and 24 hours later were euthanized under general anesthesia with the use of intravenous KCl. Hearts were removed, sectioned into 3- to 4-mm slices, and stained with 2,3,5-triphenyltetrazolium chloride (TTC) as described[22] to visualize infarcts. Fe-MSC injection sites were also identified by coadministered tissue dye. Slices were photographed on both apical and basal surfaces.

Data Analysis

Myocardial infarction was determined in vivo by DHE after Gd-DTPA infusion or ex vivo by pallor on TTC staining. The relationship between injection site and infarction was assessed qualitatively in 2 different ways. First, 3D locations of the injection sites from x-ray were displayed on DHE images with the inverse transformation of data used to perform XFM. This assumed that each injection volume of 0.4 mL would distribute as a uniform sphere centered on the position of the needle tip. Second, injected dye was visualized in relation to ex vivo TTC staining. Within each animal, injections formed vertices of complex polygons, analogous to individual stars within a constellation. In this way, corresponding locations of each injection were uniquely identified in necropsy and XFM images. For each approach, 2 observers independently classified injections as within the infarct, peri-infarct, or remote; the comparator technique was readily apparent and could not be blinded.

Quantitative accuracy of each injection was determined by comparing needle tip locations on x-ray images with the locations of the iron-induced susceptibility artifacts on T2*W-GRE images. The coordinates of the susceptibility artifacts were obtained by manually tracing the border of the artifact on each image and calculating the centroid of all the tracings for each injection. These coordinates were mapped into 3D x-ray space with the use of a second XFM registration transformation computed by matching external fiducial marker positions on the x-ray images and the second 3D MR marker acquisition. The target registration error,[23] an in vivo measurement representing the difference between the XFM-predicted and actual injection locations, was calculated as the 3D distance of the circumferential and long-axis components of the vector between end-diastolic, XFM-derived injection sites and end-diastolic susceptibility artifact on T2*W-E images (Figure 4). Because XFM guidance can only assist the operator in determining the circumferential and long-axis placement of the injection catheter and because the radial position of the needle is dependent only on the needle length and the compliance of the myocardium at that location, we ignored the radial component of the vector when calculating the target registration error.

Data are presented as mean±SD of the targeting error for each animal, as well as in a cumulative distribution plot of the targeting error for all injections. Categorical targeting errors are analyzed in aggregate with the use of a κ statistic of intermodality agreement, weighted for multiple categories.[24]

The authors had full access to the data and take full responsibility for their integrity. All authors have read and agree to the manuscript as written.

Results

Survival, Procedural Details, and Complications

We performed a total of 130 injections in 12 animals with myocardial infarctions of varying size and age in both the left anterior descending and LCX territories. Relevant procedural data are summarized in Table 1. All animals survived to the study-specified euthanasia end point 24 hours after the injection procedure.

Two procedure-related complications occurred in a single animal (weight of 34 kg, below the limit of 40 kg recommended by the injection catheter manufacturer), 3 days after LCX infarction. A small pericardial effusion that was noted on preinjection MRI grew to moderate size afterward, without MRI or hemodynamic features of tamponade. Careful postmortem inspection did not reveal an obvious myocardial perforation site. This animal also suffered sustained ventricular tachycardia, which was successfully cardioverted.

Targeting of Endomyocardial Injection

Figure 3 illustrates the 3 key features of XFM-guided endomyocardial injections with the use of our method, namely, safety (Figure 3A, 3B), targeting (Figure 3C, 3D), and accuracy (Figure 3E, 3G). The percentage of injections categorized as within remote, peri-infarct, and infarct locations showed substantial agreement between the 2 modalities (κ=0.69; Table 2), whether determined by inspection of the dye staining on postmortem heart slices or determined from XFM-derived injection locations mapped onto the DHE images. Visual inspection of these distributions also compared favorably with the susceptibility artifacts seen on the postinjection T2*W-GRE imaging (Figures 4 and 5).

Quantitative in vivo measurement of the accuracy of XFM-guided injections was performed for 64 injections in those 7 animals with suitable-quality postinjection T2*W-GRE images. In 3 other animals, T2*W-GRE imaging failed to identify susceptibility artifacts because of inadequate MSC labeling with ferumoxides, and in 2 other animals Fe-MSC were not available. The overall in vivo targeting error was 3.2±2.6 mm (interquartile range, 1.0 to 4.1). These data are presented for each animal and as a cumulative distribution plot in Figure 6. With the exclusion of the first animal, an outlier, the targeting error was 2.6±1.9 mm (interquartile range, 1.0 to 3.6), including 58 injections.

Discussion

For clinical interventional procedures, guidance systems that facilitate delivery of therapies to targets on the basis of their physiological characteristics and anatomic location might improve procedural ease, safety, and efficacy. We have demonstrated the feasibility of accurate XFM-guided endomyocardial injections in a swine model of myocardial infarction in which DHE MRI was used to define the area of infarction. This method combines the strengths of x-ray and MRI to help operators navigate devices and deliver targeted therapy to the left ventricle based on direct assessments of regional myocardial thickness and tissue character.

Our study design allowed quantitative in vivo calculation of the target registration error, a measure of the intrinsic accuracy of our targeting method, by computing the distance between the coordinates of the susceptibility artifact due to injected Fe-MSC and the XFM-determined injection location for each injection. The average target registration error was 3.2±2.6 mm, and 75% of our injections were within 4.1 mm of the XFM-predicted location. We are not aware of any comparable in vivo measurements of target registration error in the heart. We performed our measurement of target registration error by comparing injection needle positions with the location of corresponding iron-induced susceptibility artifacts on T2*W-GRE imaging rather than by comparing positions with the location of dye stains on the ex vivo TTC-stained heart

slices. Ex vivo measurements of the distance of injection sites marked by dye staining to the infarct border on TTC-stained heart slices are difficult to quantify accurately for the following reasons. Myocardial wall thickness and cardiac dimensions are significantly altered postmortem. During intramyocardial injection, most injectate disperses via venous, lymphatic, and intracavitary routes,[25] which may cause dye dispersion away from the original injection site and produce the areas of confluent tissue dye staining observed ex vivo, confounding localization of discrete injection sites. In addition, it is difficult to precisely localize injection sites on surfaces of heart slices alone, especially in instances in which, in a given slice, the injection might span the cut surfaces. This makes it difficult to compare the target registration error data reported in the present study with previous reports[26]; therefore, we performed the qualitative analysis summarized in Table 2.

In the present study, we fused static end-diastolic images of MRI-derived contours onto real-time x-ray throughout the cardiac cycle. Alternatively, we could "flash" overlay the ECG-gated MRI data only during the appropriate phase of the cardiac cycle during x-ray. For the purpose of demonstration, in 1 animal we fused ECG-gated, MRI-derived contours from multiple phases of the cardiac cycle onto matching phases of the cardiac cycle under x-ray (see online-only Data Supplement). This technique might further reduce targeting error.

A novel feature of XFM guidance is the use of a global map of left ventricular myocardial thickness in addition to the display of the infarct location during navigation and selection of an injection site. The thickness of the myocardial wall that can be injected safely varies according to the needle length of the injection system. The manufacturer of the injection system used in the present study suggested that myocardial thickness be at least 6 mm wherever injections are undertaken. The myocardial thickness map gives the operator a "go/no go" picture of the left ventricular endocardial surface by coloring regions with a safe myocardial thickness in green and unsafe regions in red. The safety threshold can be varied depending on the device chosen and may therefore be applied to different injection systems.

Our registration system can be implemented across vendor platforms. MR data are transferred in Digital Imaging and Communications in Medicine (DICOM) standard format. Real-time x-ray fluoroscopy data are captured with a video frame grabber or might be obtained directly from the vendor digital image chain. The only vendor-specific elements of our system are the components that query the x-ray system for gantry and table position. These software subsystems could be customized for any vendor. In the future, our methodology, with the use of external fiducial markers to register images within a combined x-ray/MRI suite, could be applied to noncontiguous x-ray and MRI systems, as long as the fiducial markers are not displaced.

Comparison With Other MRI- or Computer Tomography–Based Methods

Our XFM system combines prior 3D data derived from MRI with real-time 2D projection data from live x-ray fluoroscopy. It has enhanced registration accuracy compared with simple superposition because it encompasses distortion correction for pincushion and sigmoidal error in the image intensifier–based x-ray images; gradient warp error in the MR images; and correction for varying x-ray FOV, gantry position, and table position. Other investigators have used less extensive multimodality image registration systems in catheter-based cardiovascular procedures.[27–31]

In an imaging phantom, our system produces a target registration error of 0.99 mm.[17] This compares favorably with target registration error measurements in a phantom made by Reddy and colleagues[26] of 1.2 mm in a system combining prior MRI with electroanatomic-guided catheter injections and by Rhode and colleagues[32] of 2.55 mm in a combined x-ray/MRI system using optical tracking of the patient table to register prior MRI with real-time projection,

x-ray–guided injections. The experiments by Reddy and colleagues had the advantage of seeking to ablate specific myocardial targets created with prior iron injections mapped from MRI onto their electroanatomic guidance system. Their approach may be limited because natural catheter and myocardium geometries might favor initial targets to which the catheter intrinsically returns during the follow-up ablation experiment, exaggerating precision. We instead targeted infarct borders in an effort to avoid this catheter-geometry bias. The approach by Rhode and colleagues has the advantage of requiring no image segmentation or image-similarity computation to accomplish the registration. However, their method registers the imaging systems independent of the patient. Therefore, patient motion disrupts the image registration. Our system allows for updating registration due to patient movement because the registration is based on patient-specific markers. Moreover, Rhode and colleagues characterized the target registration error only for phantom experiments.

Real-time interventional MRI[2] is an attractive alternate approach for myocardial injection but is limited by the unavailability of conspicuous clinical-grade devices. This approach would otherwise be superior in that infarct and myocardial thickness can be displayed in real time rather than as a previously acquired roadmap, as in this study.

Comparison With Other Guidance Methods

Targeted endomyocardial injections have been performed with a number of guidance systems, including electroanatomic mapping[3,4,7,9,11–13,33,34] and intracardiac[14] and 3D surface echocardiography.[35]

To date, electroanatomic mapping has provided the mainstay for targeting injection.[3,4,7,9, 11–13,33,34] In this technique, the 3D position of a custom catheter is located by automated analysis of the currents induced in the catheter tip as it moves within 3 intersecting magnetic fields surrounding the patient. At each point, endocardial voltage or periodic motion of the catheter tip can be recorded. From a fluoroscopically determined anatomic reference point, the catheter is moved along the endocardial surface to record multiple points. In general, multiple measurements are required to provide an adequate interpolated 3D map, usually color coded according to the measured unipolar voltage. This can make electroanatomic mapping time-consuming, even in experienced hands, although newer iterations may make the process less laborious. Electroanatomic mapping does not provide direct assessment of myocardial wall thickness to the operator during the procedure. Furthermore, thresholds of unipolar voltage thought to represent myocardial viability are controversial.[36,37] The ability of this technique to identify areas of hypoperfusion and myocardial viability does not consistently compare well with conventional imaging techniques.[38,39] Consequently, considerable expertise and experience are required to interpret these maps reliably. Mapping confers incremental risk,[9] requires multiple steps, and appears to provide less structural information than MRI.

Both intracardiac[14] and 3D[35] echocardiographic techniques have been used to determine the success of endomyocardial injections. Both have been used in conjunction with x-ray. Apposition of the catheter to the endocardium in real time can be visualized directly, and mixing the injectate with echo contrast can provide direct confirmation of the success of injection. In addition, the temporal resolution offered by echocardiography provides real-time determination of the myocardial wall thickness at injection sites and immediate identification of injection-related complications. These approaches are promising but are currently limited by their inability to provide complete volumetric imaging of the heart.

Conclusion

We report the successful application of external fiducial marker–based 3D to 2D registration and fusion of x-ray and MR images for targeted endomyocardial injection in a model of

myocardial infarction. The target registration error was 3.2±2.6 mm, with 75% of injections within 4.1 mm of the XFM-predicted location. Our approach likely can be applied without the need for a combined x-ray/MRI suite, without additional optical tracking or electroanatomic mapping hard-ware, and does not restrict operators in their choice of catheters or devices. It is potentially generalizable to other endovascular applications and can be combined with electroanatomic mapping, if desired. The present data suggest that the safety and efficacy of this approach for performing targeted endomyocardial delivery should be evaluated further in the clinical setting.

CLINICAL PERSPECTIVE

Magnetic resonance imaging (MRI) provides superb imaging of heart function and pathology, but MRI-guided interventional procedures remain technically challenging for want of clinical-grade catheter devices. X-ray fluoroscopy, despite its high temporal and spatial resolution, provides only limited depiction of myocardial viability and function and appears inadequate to guide spatially precise myocardial injections. With the use of skin markers to register image data from the 2 separate imaging modalities and to correct for patient movement, this work combines 3-dimensional features of interest with real-time 2-dimensional x-ray imaging, called x-ray fused with MRI (XFM). This report demonstrates the feasibility of accurate XFM-guided endomyocardial injections in a pig model of myocardial infarction. The x-ray permits simple manipulation of injection catheters; the superimposed MRI data provide information about the spatial position of the myocardial infarcts and about the location of “danger zones” where the myocardium is considered too thin for safe injection. This method combines the strengths of x-ray and MRI to help operators navigate devices and deliver targeted therapy to the left ventricle. XFM may have other applications in enhancing the x-ray–guided catheter treatment of heart disease.

Supplementary Material

Refer to Web version on PubMed Central for supplementary material.

Acknowledgements

We thank Victor J. Wright, William H. Schenke, Joni Taylor, Kathryn Hope, Katherine Lucas, and Karena M. Gildea for technical assistance; Stephanie Webber, Wendy Naimark, Erik Sperry, and Maria Palasis of Boston Scientific Corporation for providing Stilletto injection systems; Stasia A. Anderson, Naheed Banu, and Joseph A. Frank for cell processing; and Peter Kellman for the phase-sensitive inversion recovery pulse sequence.

Sources of Funding

This work was supported by National Institutes of Health grants Z01-HL004608-06 (Dr McVeigh) and Z01-HL005062-04 (Dr Lederman).

References

1. Dohmann HF, Perin EC, Takiya CM, Silva GV, Silva SA, Sousa AL, Mesquita CT, Rossi MI, Pascarelli BM, Assis IM, Dutra HS, Assad JA, Castello-Branco RV, Drummond C, Dohmann HJ, Willerson JT, Borojevic R. Transendocardial autologous bone marrow mononuclear cell injection in ischemic heart failure: postmortem anatomicopathologic and immunohistochemical findings. Circulation 2005;112:521–526. [PubMed: 16027258]
2. Dick AJ, Guttman MA, Raman VK, Peters DC, Pessanha BS, Hill JM, Smith S, Scott G, McVeigh ER, Lederman RJ. Magnetic resonance fluoroscopy allows targeted delivery of mesenchymal stem cells to infarct borders in swine. Circulation 2003;108:2899–2904. [PubMed: 14656911]
3. Kawamoto A, Tkebuchava T, Yamaguchi J, Nishimura H, Yoon YS, Milliken C, Uchida S, Masuo O, Iwaguro H, Ma H, Hanley A, Silver M, Kearney M, Losordo DW, Isner JM, Asahara T. Intramyocardial

transplantation of autologous endothelial progenitor cells for therapeutic neo-vascularization of myocardial ischemia. Circulation 2003;107:461–468. [PubMed: 12551872]

4. Perin EC, Dohmann HF, Borojevic R, Silva SA, Sousa AL, Mesquita CT, Rossi MI, Carvalho AC, Dutra HS, Dohmann HJ, Silva GV, Belem L, Vivacqua R, Rangel FO, Esporcatte R, Geng YJ, Vaughn WK, Assad JA, Mesquita ET, Willerson JT. Transendocardial, autologous bone marrow cell transplantation for severe, chronic ischemic heart failure. Circulation 2003;107:2294–2302. [PubMed: 12707230]
5. Chazaud B, Hittinger L, Sonnet C, Champagne S, Le Corvoisier P, Benhaiem-Sigaux N, Unterseeh T, Su J, Merlet P, Rahmouni A, Garot J, Gherardi R, Teiger E. Endoventricular porcine autologous myoblast transplantation can be successfully achieved with minor mechanical cell damage. Cardiovasc Res 2003;58:444–450. [PubMed: 12757878]
6. Smits PC, van Geuns RJ, Poldermans D, Bountioukos M, Onderwater EE, Lee CH, Maat AP, Serruys PW. Catheter-based intramyocardial injection of autologous skeletal myoblasts as a primary treatment of ischemic heart failure: clinical experience with six-month follow-up. J Am Coll Cardiol 2003;42:2063–2069. [PubMed: 14680727]
7. Tse HF, Kwong YL, Chan JK, Lo G, Ho CL, Lau CP. Angiogenesis in ischaemic myocardium by intramyocardial autologous bone marrow mononuclear cell implantation. Lancet 2003;361:47–49. [PubMed: 12517468]
8. Kamihata H, Matsubara H, Nishiue T, Fujiyama S, Amano K, Iba O, Imada T, Iwasaka T. Improvement of collateral perfusion and regional function by implantation of peripheral blood mononuclear cells into ischemic hibernating myocardium. Arterioscler Thromb Vasc Biol 2002;22:1804–1810. [PubMed: 12426208]
9. Kastrup J, Jorgensen E, Ruck A, Tagil K, Glogar D, Ruzyllo W, Botker HE, Dudek D, Drvota V, Hesse B, Thuesen L, Blomberg P, Gyongyosi M, Sylven C. Direct intramyocardial plasmid vascular endothelial growth factor-A165 gene therapy in patients with stable severe angina pectoris: a randomized double-blind placebo-controlled study: the Euroinject One trial. J Am Coll Cardiol 2005;45:982–988. [PubMed: 15808751]
10. Rutanen J, Rissanen TT, Markkanen JE, Gruchala M, Silvennoinen P, Kivela A, Hedman A, Hedman M, Heikura T, Orden MR, Stacker SA, Achen MG, Hartikainen J, Yla-Herttuala S. Adenoviral catheter-mediated intramyocardial gene transfer using the mature form of vascular endothelial growth factor-D induces transmural angiogenesis in porcine heart. Circulation 2004;109:1029–1035. [PubMed: 14967735]
11. Losordo DW, Vale PR, Hendel RC, Milliken CE, Fortuin FD, Cummings N, Schatz RA, Asahara T, Isner JM, Kuntz RE. Phase 1/2 placebo-controlled, double-blind, dose-escalating trial of myocardial vascular endothelial growth factor 2 gene transfer by catheter delivery in patients with chronic myocardial ischemia. Circulation 2002;105:2012–2018. [PubMed: 11980678]
12. Vale PR, Losordo DW, Milliken CE, McDonald MC, Gravelin LM, Curry CM, Esakof DD, Maysky M, Symes JF, Isner JM. Randomized, single-blind, placebo-controlled pilot study of catheter-based myocardial gene transfer for therapeutic angiogenesis using left ventricular electromechanical mapping in patients with chronic myocardial ischemia. Circulation 2001;103:2138–2143. [PubMed: 11331253]
13. Vale PR, Losordo DW, Milliken CE, Maysky M, Esakof DD, Symes JF, Isner JM. Left ventricular electromechanical mapping to assess efficacy of phVEGF(165) gene transfer for therapeutic angiogenesis in chronic myocardial ischemia. Circulation 2000;102:965–974. [PubMed: 10961959]
14. Park SW, Gwon HC, Jeong JO, Byun J, Kang HS, You JR, Cho SS, Lee MJ, Lee Y, Kim S, Kim DK. Intracardiac echocardiographic guidance and monitoring during percutaneous endomyocardial gene injection in porcine heart. Hum Gene Ther 2001;12:893–903. [PubMed: 11387055]
15. McVeigh ER. MRI of myocardial function: motion tracking techniques. Magn Reson Imaging 1996;14:137–150. [PubMed: 8847969]
16. Kim RJ, Wu E, Rafael A, Chen EL, Parker MA, Simonetti O, Klocke FJ, Bonow RO, Judd RM. The use of contrast-enhanced magnetic resonance imaging to identify reversible myocardial dysfunction. N Engl J Med 2000;343:1445–1453. [PubMed: 11078769]
17. Gutierrez LF, Schechter G, Lederman RJ, McVeigh ER, Ozturk C. Distortion correction, calibration and registration: toward an integrated MR and X-ray interventional suite. Proc SPIE 2005;5744:146–156.

18. Arbab AS, Yocum GT, Kalish H, Jordan EK, Anderson SA, Khakoo AY, Read EJ, Frank JA. Efficient magnetic cell labeling with protamine sulfate complexed to ferumoxides for cellular MRI. Blood 2004;104:1217–1223. [PubMed: 15100158]
19. Kellman P, Arai AE, McVeigh ER, Aletras AH. Phase-sensitive inversion recovery for detecting myocardial infarction using gadolinium-delayed hyperenhancement. Magn Reson Med 2002;47:372–383. [PubMed: 11810682]
20. Jovicich J, Czanner S, Greve D, Haley E, van der Kouwe A, Gollub R, Kennedy D, Schmitt F, Brown G, Macfall J, Fischl B, Dale A. Reliability in multi-site structural MRI studies: effects of gradient non-linearity correction on phantom and human data. Neuroimage 2006;30:436–443. [PubMed: 16300968]
21. Ozturk C, McVeigh ER. Four-dimensional B-spline based motion analysis of tagged MR images: introduction and in vivo validation. Phys Med Biol 2000;45:1683–1702. [PubMed: 10870718]
22. Fishbein MC, Meerbaum S, Rit J, Lando U, Kanmatsuse K, Mercier JC, Corday E, Ganz W. Early phase acute myocardial infarct size quantification: validation of the triphenyl tetrazolium chloride tissue enzyme staining technique. Am Heart J 1981;101:593–600. [PubMed: 6164281]
23. Fitzpatrick JM, West JB, Maurer CR Jr. Predicting error in rigid-body point-based registration. IEEE Trans Med Imaging 1998;17:694–702. [PubMed: 9874293]
24. Kundel HL, Polansky M. Measurement of observer agreement. Radiology 2003;228:303–308. [PubMed: 12819342]
25. Grossman PM, Han Z, Palasis M, Barry JJ, Lederman RJ. Incomplete retention after direct myocardial injection. Catheter Cardiovasc Interv 2002;55:392–397. [PubMed: 11870950]
26. Reddy VY, Malchano ZJ, Holmvang G, Schmidt EJ, d'Avila A, Houghtaling C, Chan RC, Ruskin JN. Integration of cardiac magnetic resonance imaging with three-dimensional electroanatomic mapping to guide left ventricular catheter manipulation: feasibility in a porcine model of healed myocardial infarction. J Am Coll Cardiol 2004;44:2202–2213. [PubMed: 15582319]
27. Dickfeld T, Calkins H, Zviman M, Kato R, Meininger G, Lickfett L, Berger R, Halperin H, Solomon SB. Anatomic stereotactic catheter ablation on three-dimensional magnetic resonance images in real time. Circulation 2003;108:2407–2413. [PubMed: 14568905]
28. Ector J, De Buck S, Adams J, Dymarkowski S, Bogaert J, Maes F, Heidbuchel H. Cardiac three-dimensional magnetic resonance imaging and fluoroscopy merging: a new approach for electroanatomic mapping to assist catheter ablation. Circulation 2005;112:3769–3776. [PubMed: 16330683]
29. Sra J, Krum D, Malloy A, Vass M, Belanger B, Soubelet E, Vaillant R, Akhtar M. Registration of three-dimensional left atrial computed tomographic images with projection images obtained using fluoroscopy. Circulation 2005;112:3763–3768. [PubMed: 16344405]
30. Tops LF, Bax JJ, Zeppenfeld K, Jongbloed MR, Lamb HJ, van der Wall EE, Schalij MJ. Fusion of multislice computed tomography imaging with three-dimensional electroanatomic mapping to guide radiofrequency catheter ablation procedures. Heart Rhythm 2005;2:1076–1081. [PubMed: 16188585]
31. Dong J, Calkins H, Solomon SB, Lai S, Dalal D, Lardo A, Brem E, Preiss A, Berger RD, Halperin H, Dickfeld T. Integrated electroanatomic mapping with three-dimensional computed tomographic images for real-time guided ablations. Circulation 2006;113:186–194. [PubMed: 16401772]
32. Rhode KS, Hill DL, Edwards PJ, Hipwell J, Rueckert D, Sanchez-Ortiz G, Hegde S, Rahunathan V, Razavi R. Registration and tracking to integrate X-ray and MR images in an XMR facility. IEEE Trans Med Imaging 2003;22:1369–1378. [PubMed: 14606671]
33. Kornowski R, Hong MK, Gepstein L, Goldstein S, Ellahham S, Ben-Haim SA, Leon MB. Preliminary animal and clinical experiences using an electromechanical endocardial mapping procedure to distinguish infarcted from healthy myocardium. Circulation 1998;98:1116–1124. [PubMed: 9736599]
34. Smits PC, van Langenhove G, Schaar M, Reijs A, Bakker WH, van der Giessen WJ, Verdouw PD, Krenning EP, Serruys PW. Efficacy of percutaneous intramyocardial injections using a nonfluoroscopic 3-D mapping based catheter system. Cardiovasc Drugs Ther 2002;16:527–533. [PubMed: 12766387]

35. Baklanov DV, de Muinck ED, Simons M, Moodie KL, Arbuckle BE, Thompson CA, Palac RT. Live 3D echo guidance of catheter-based endomyocardial injection. Catheter Cardiovasc Interv 2005;65:340–345. [PubMed: 15832326]

36. Mayes CE Jr, Bashore TM. Biosensibility of viability: NOGA or no good? Catheter Cardiovasc Interv 2001;52:348–350. [PubMed: 11246250]

37. Fallavollita JA, Valeti U, Oza S, Canty JM Jr. Spatial heterogeneity of endocardial voltage amplitude in viable, chronically dysfunctional myocardium. Basic Res Cardiol 2004;99:212–222. [PubMed: 15088106]

38. Graf S, Gyongyosi M, Khorsand A, Nekolla SG, Pirich C, Kletter K, Dudczak R, Glogar D, Porenta G, Sochor H. Electromechanical properties of perfusion/metabolism mismatch: comparison of nonfluoroscopic electroanatomic mapping with 18F-FDG PET. J Nucl Med 2004;45:1611–1618. [PubMed: 15471823]

39. Wiggers H, Botker HE, Sogaard P, Kaltoft A, Hermansen F, Kim WY, Krusell L, Thuesen L. Electromechanical mapping versus positron emission tomography and single photon emission computed tomography for the detection of myocardial viability in patients with ischemic cardiomyopathy. J Am Coll Cardiol 2003;41:843–848. [PubMed: 12628732]

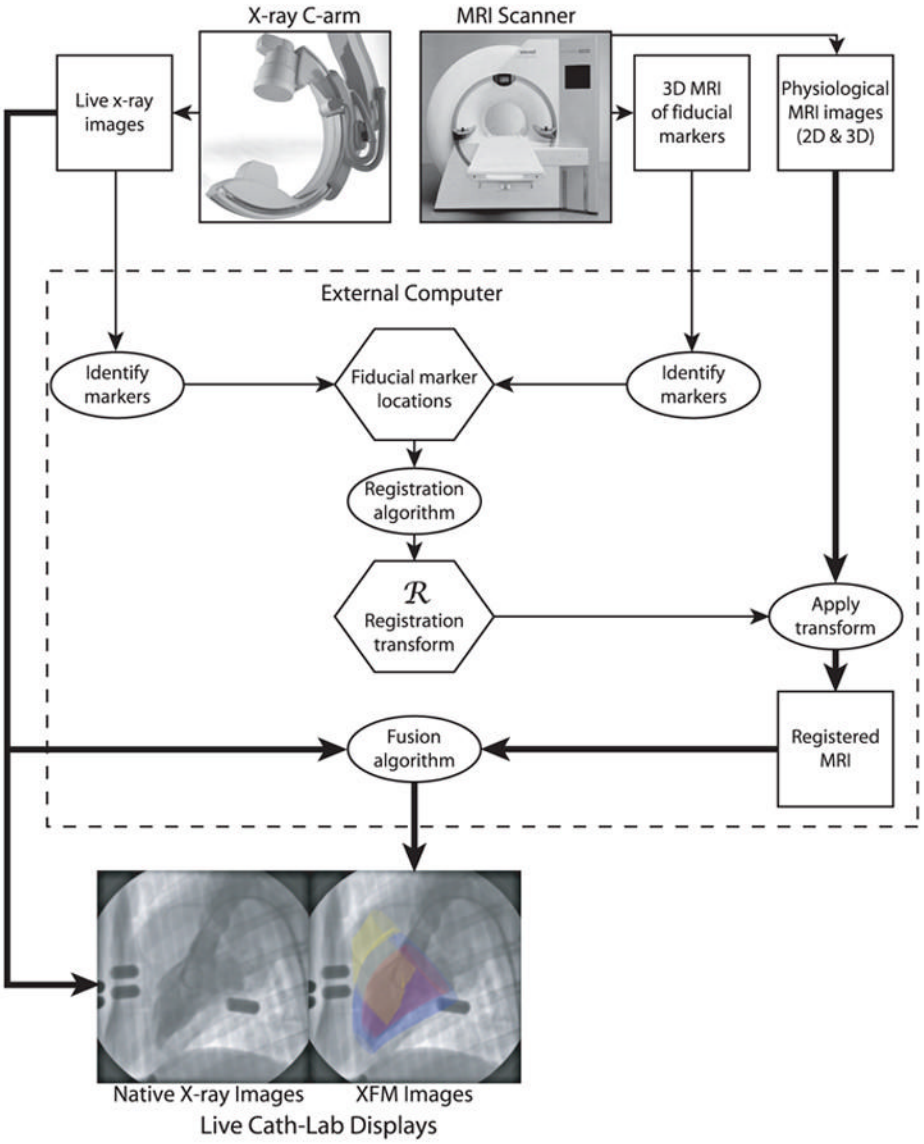

Figure 1.
Schematic illustration of the components of XFM using external fiducial markers. In the example XFM image, the left ventricular endocardium is depicted in red, left ventricular epicardium in blue, and right ventricular endocardium in yellow.

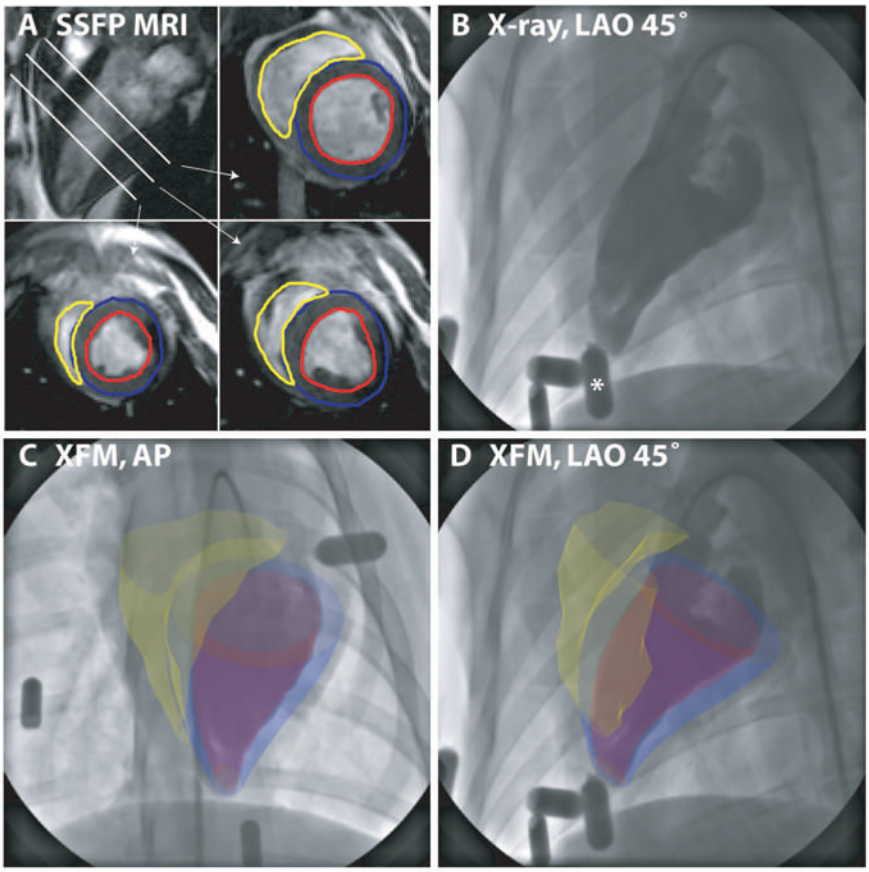

Figure 2.
Fusion of 3D MRI-derived surfaces with radiocontrast ventriculograms. End-diastolic short-axis SSFP images from apex to base are segmented to define left ventricular endocardial (red), left ventricular epicardial (blue), and right ventricular endocardial (yellow) contours (A). Three-dimensional surfaces are generated from these contours as described in the text and overlaid on the live x-ray display during ventriculography (B) (The asterisk denotes the external fiducial marker) acquired in anteroposterior (AP) (C) and left anterior oblique (LAO) 45° (D) projections.

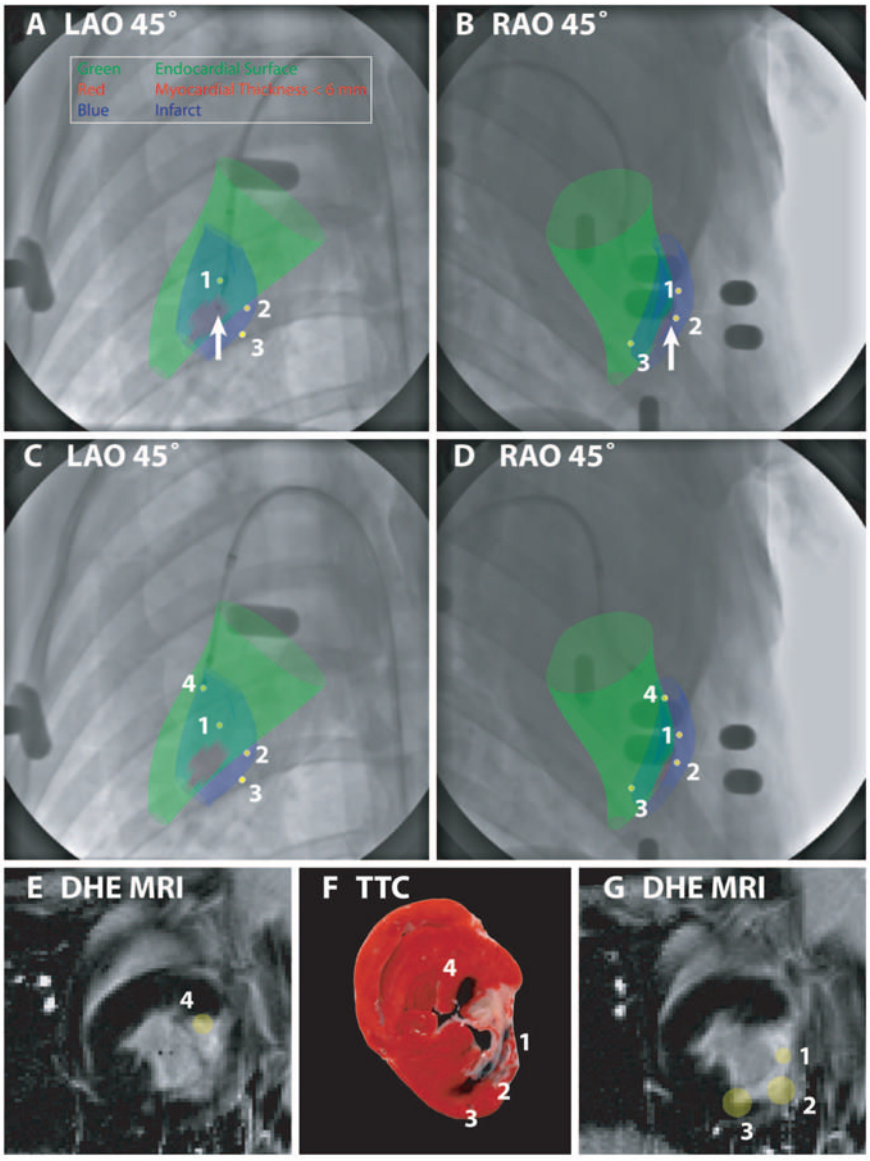

Figure 3.

XFM targeting of endomyocardial injections according to infarct location (blue surface) and regional myocardial wall thickness (colored green for wall thickness >6 mm and red for wall thickness ≤6 mm) in an animal with a chronic LCX infarct. These surfaces were displayed over x-ray in orthogonal projections (A and B). The catheter is positioned where the wall thickness is ≤6 mm (arrow); this location was therefore rejected. C and D demonstrate relocation of the injection catheter to a "safe" peri-infarct location with wall thickness >6 mm. After deployment of the needle, orthogonal x-ray views allow reconstruction of the injection location in 3D (yellow spot, numbered 4). Previous injection locations (yellow spots, numbered 1 to 3) are also displayed to help avoid overlapping injections. The 3D injection locations are also displayed superimposed on the prior DHE MRI (E and G). A postmortem TTC-stained heart slice (F), located between the MRI slices displayed in E and G, shows tissue dye–staining patterns that correlate well with the XFM-derived injection locations.

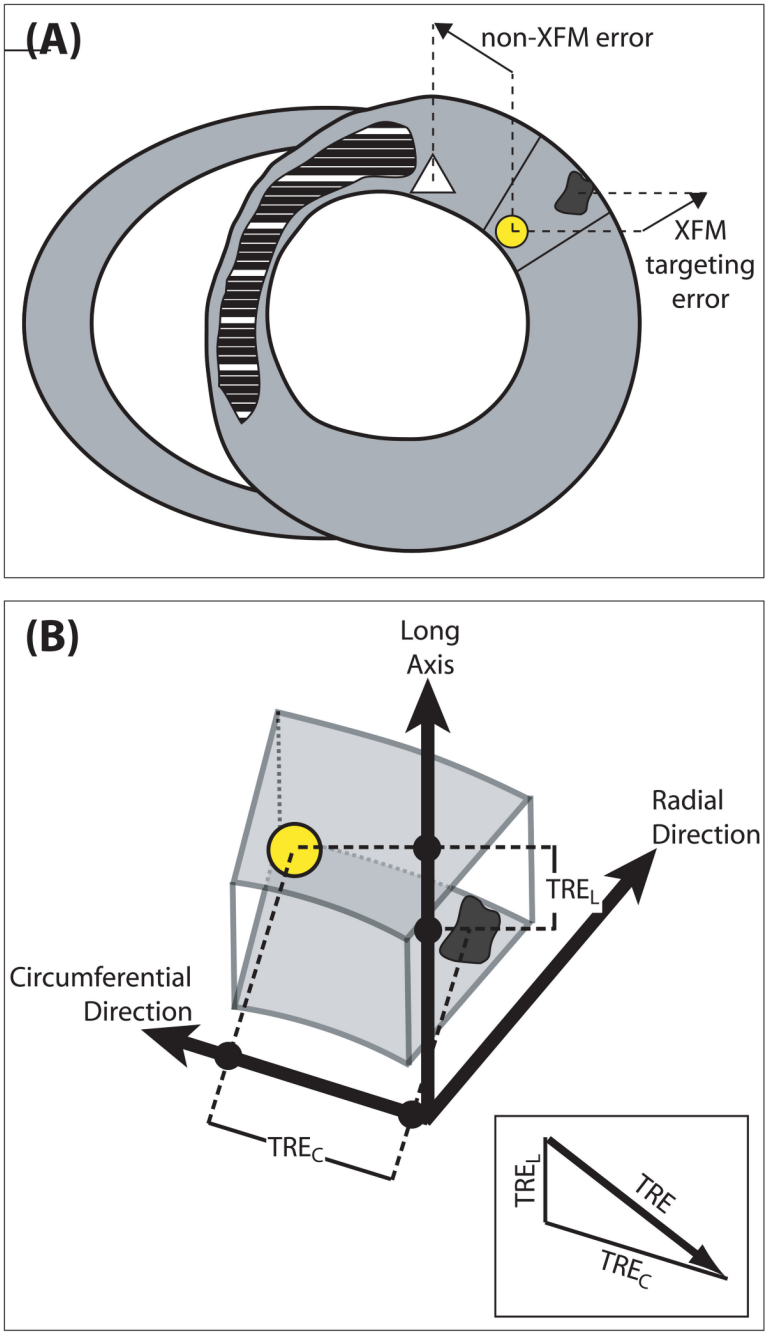

Figure 4.

A, Schematic short-axis slice, with normal myocardium in gray and the infarct in cross-hatch. The yellow spot represents an XFM-predicted injection location. The dark spot represents the susceptibility artifact on T2*W-GRE imaging due to injected Fe-MSC. The white triangle denotes an ideal target. The distance between the white triangle and the yellow dot represents errors due to device and operator factors, whereas the distance between the yellow dot and dark spot represents intrinsic targeting errors of our registration method. B, Calculation of the target registration error (TRE). A 3D vector relates the end-diastolic XFM-derived injection location (yellow) and the centroid of the corresponding iron injection (black) on the postinjection end-diastolic T2*W-GRE MRI images. The target registration error is the length of the

circumferential (TREC) and long-axis (TREL) components of this vector. The radial component of the vector, which is not controlled by the operator, is ignored (see text).

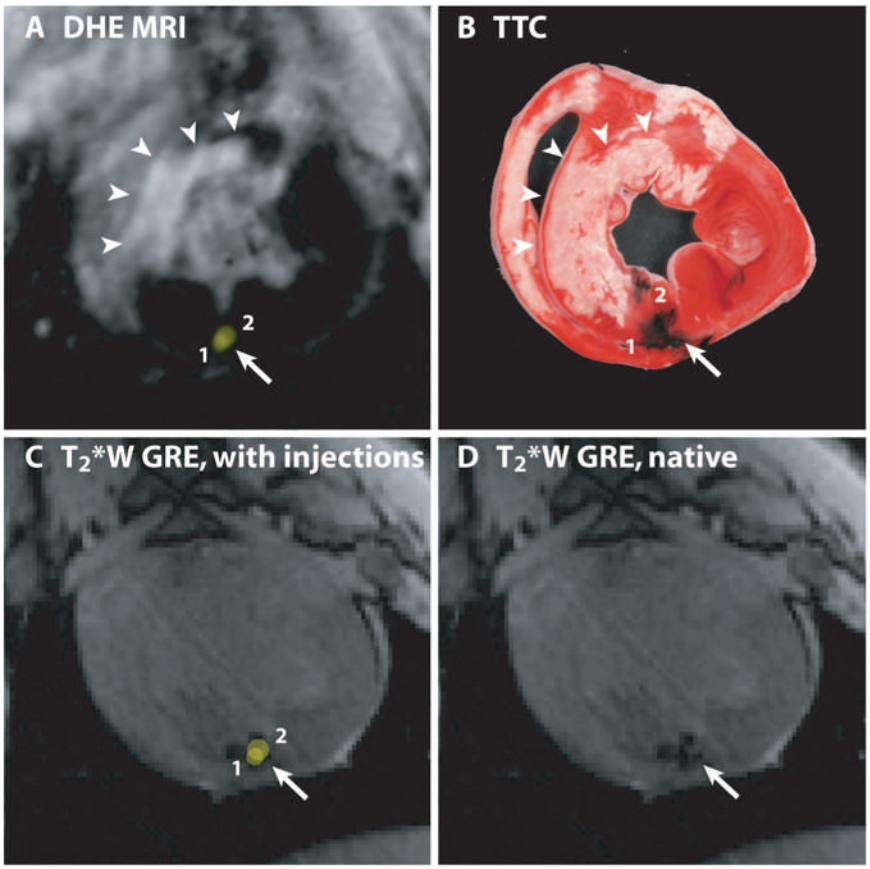

Figure 5.

The locations of 2 XFM-guided injections of Fe-MSC mixed with tissue dye are shown relative to areas of infarction demonstrated in vivo by DHE MRI (A) and ex vivo by TTC staining (B). The XFM-guided injection locations (yellow spots, numbered 1 and 2) are superimposed on the preinjection DHE-MR to target injections (A) and on the postinjection T2*W GRE image (C) to validate in vivo accuracy of XFM-guided injection locations. The susceptibility artifact on this image resulting from injected Fe-MSC is better appreciated in D. The distributions of tissue dye stains on the TTC-stained heart slice (B) and susceptibility artifacts (D) are very similar.

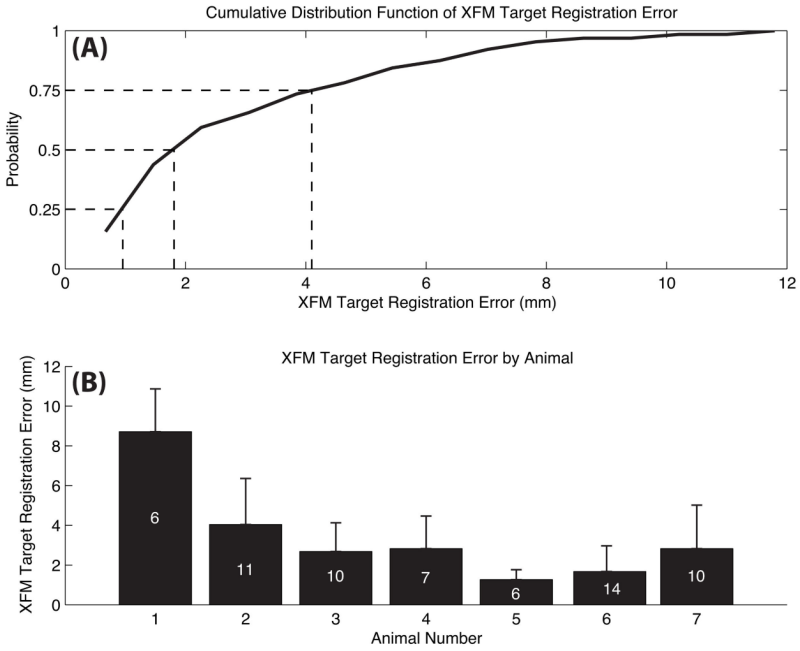

Figure 6.

In vivo validation of XFM-guided targeting accuracy. A, Cumulative distribution function of target registration errors of all 64 injections performed in 7 animals with evaluable data. B, Mean±SD target registration error for each animal independently. The number within bars indicates the number of injections in each individual animal.

TABLE 1

Procedural Data

Animal weight, kg*	45.4±6.7
No. of injections per animal*	10.7±3.0
Procedure time per injection, min*	3.3±1.1
Fluoroscopy time per injection, min*	1.3±0.3
Range of myocardial thickness, mm	2.6–17.7
Age of myocardial infarcts, d	3–74 (median, 17.5)

* Data are mean±SD.

TABLE 2

Injection Location Classification Relative to Infarct as Determined by XFM and Ex Vivo Analysis in 9 Animals

	Ex Vivo Analysis			
	Within Infarct	**Peri-Infarct**	**Remote**	**Total**
XFM				
Within infarct	16	7	1	24
Peri-infarct	4	29	4	37
Remote	3	1	23	27
Total	23	37	28	88

The weighted κ statistic, reflecting the agreement between the 2 modalities, was 0.69.